Analyst

PAPER

View Article Online
View Journal | View Issue

Cite this: *Analyst*, 2015, **140**, 1166

Citrate-capped gold nanoparticles for the label-free detection of ubiquitin C-terminal hydrolase-1†

Srishti Agarwal,‡[a] Priyanka Mishra,‡[a] Gururaj Shivange,[a] Naveena Kodipelli,[a] María Moros,[b] Jesús M. de la Fuente[b] and Roy Anindya*[a]

Ubiquitin C-terminal hydrolase-1 (UCH-L1) is a specific neuronal endoprotease that cleaves the specific peptide bond between ubiquitin molecules. UCH-L1 is released in serum and cerebrospinal fluid after severe brain injury and is considered to be an important biomarker of brain injury. A common polymorphism of UCH-L1 (S18Y) is also linked to a reduced risk of Parkinson's disease. In addition to its function in neuronal tissues, UCH-L1 may also play a part in the progression of certain non-neuronal cancers. UCH-L1 is highly expressed in primary lung tumors and colo-rectal cancers, suggesting a role in tumorigenesis. We report here the development of a sensitive and accurate UCH-L1 assay based on the surface plasmon resonance (SPR) absorbance of gold nanoparticles. We created a unique UCH-L1 substrate containing a ubiquitin molecule with two terminal thiol groups. This UCH-L1 substrate interacted with gold nanoparticles *via* the terminal thiol groups and induced clustering of the nanoparticles, which was detected by SPR absorbance at 650 nm. UCH-L1 proteolytically cleaved the substrate and the clustered gold nanoparticles were dispersed and could be detected by a shift in the SPR absorbance to 530 nm. This change in absorbance was proportional to the concentration of UCH-L1 and can be used for the quantification of functional UCH-L1. The currently available fluorescence-based UCH-L1 assay is affected by a high background signal and a poor detection limit, especially in the presence of serum. The assay reported here can detect concentrations of UCH-L1 as low as 20 ng ml^{-1} (0.8 nM) and the presence of serum had no effect on the detection limit. This assay could be adapted for the rapid determination of the severity of brain injury and could also be applied to high-throughput screening of inhibitors of UCH-L1 enzymatic activity in Parkinson's disease and cancer.

Received 23rd October 2014,
Accepted 5th December 2014

DOI: 10.1039/c4an01935k

www.rsc.org/analyst

1. Introduction

Ubiquitin is a polypeptide found in all eukaryotes and is made up of 76 amino acids. The covalent attachment of ubiquitin to cellular proteins targets them for proteasomal degradation. In contrast, deubiquitination reverses the ubiquitination process and is carried out by deubiquitinating enzymes. Based on sequence similarity, deubiquitinating enzymes have been classified into ubiquitin C-terminal hydrolases (UCHs) and ubiquitin-specific proteases. Both classes are thiol proteases that hydrolyze the isopeptide bond between the substrate and the C-terminal glycine 76 of ubiquitin. Similar to the papain family of cysteine proteases, the active site catalytic triad of the UCH family of deubiquitinating enzymes consists of cysteine, histidine and aspartate.

To date, four UCH enzymes have been identified in human cells: UCH-L1, UCH-L3, UCH-L5 and BRCA1-associated protein 1. Of these enzymes, UCH-L1 is a highly specific neuronal protein concentrated in the grey matter region of the brain.[1] This 24 kDa enzyme constitutes 10% of neuronal proteins.[2] The physiological role of UCH-L1 is to process a polyubiquitin precursor that is important for the turnover of proteins in neurons. Human studies have also linked UCH-L1 to degenerative central nervous system diseases such as Parkinson's disease and Alzheimer's disease.[3] UCH-L1 has also been shown to be a biomarker of neuronal loss during brain hemorrhage.[4] Previous studies have established a few protein biomarkers for brain injury.[5,6] These include neuron-specific enolase (NSE), glial protein S-100β, myelin basic protein and

[a]*Department of Biotechnology, Indian Institute of Technology Hyderabad, Ordnance Factory Estate, Yeddumailaram-502205, Hyderabad, India.*
E-mail: anindya@iith.ac.in; Fax: +91-40-23016032; Tel: +91-40-23016083
[b]*Nanotherapy and Nanodiagnostics Group, Instituto de Nanociencia de Aragón (INA), Universidad de Zaragoza, Zaragoza, Spain*
†Electronic supplementary information (ESI) available. See DOI: 10.1039/c4an01935k
‡These authors contributed equally.

UCH-L1.[7–10] Although NSE, S100β and myelin basic protein have been shown to be released in the blood following brain damage, conflicting results make their use as biomarkers uncertain.[11,12] In contrast, UCHL-1 protein is present exclusively in neurons (unlike NSE and S100B, which are also present in non-neural tissues).[10] UCHL-1 (also known as PGP 9.5) was first detected as a brain-specific protein over 30 years ago.[2] It has been shown that UCHL-1 is released in cerebrospinal fluid after ischemic and traumatic brain injury in rats.[13] UCH-L1 has recently been discovered in cerebrospinal fluid after serious brain injury and clinical studies have established a strong correlation between the concentration of UCH-L1 and the outcome of treatment.[14–16] As severe head injury that damages internal brain tissues is a leading cause of death and disability, a simple and inexpensive assay to determine UCH-L1 in clinical samples would help doctors to quickly determine the severity of brain damage in patients, monitor the progress of treatment and ultimately predict the chance of survival.

Although the expression of UCH-L1 is normally limited to neuronal tissues,[17] UCH-L1 levels have been found to be increased in various malignancies, including acute lymphoblastic leukemia, breast cancer, leukemia, medullary thyroid carcinoma, non-small cell lung cancer, neuroblastoma, and in prostate, esophageal, colo-rectal and pancreatic cancer, indicating the involvement of UCHL-1 as an oncogene in the pathogenesis of these tumors.[18–27] This positive correlation between UCH-L1 and tumor progression suggests that UCH-L1 may play a part in cancer tumorigenesis. UCH-L1 has also been shown to be induced as a response to tumor growth and its expression has an antiproliferative effect.[28] As a result of the up-regulation of UCH-L1 in many cancer tissues, high levels of UCH-L1, particularly in non-neuronal tissues, may serve as an early detection biomarker for tumors. Interestingly, UCH-L1 itself could be a potential therapeutic target for the treatment of cancer.[28] A functional UCH-L1 assay that can be adapted to a high-throughput setting would therefore be useful in screening inhibitors. Moreover, a simple assay to quantify UCHL-1 directly from clinical samples would help in cancer staging and treatment at the time of diagnosis and could ultimately improve patient care.

Our decision to develop an assay based on gold nanoparticles was inspired by the study of Guarise *et al.*,[29] who showed that citrate-stabilized gold nanoparticles interact strongly with head and tail thiol groups containing peptides, causing the gold nanoparticles to form clusters. Gold nanoparticles about 30 nm in diameter absorb at 530 nm as a result of the excitation of surface plasmons, which shift to longer wavelengths (650 nm) when aggregates form. The progress of aggregate formation can be followed with the naked eye as the color of the solution changes from red to blue. Such a clear color change during the aggregation or dispersion of gold nanoparticles provides an elegant platform on which to develop an absorption-based colorimetric detection system without the requirement of sophisticated instrumentation. The possibility of controlling nanoparticle aggregation has been exploited in many areas of chemical sensing and enzyme bioassays. Studies using gold nanoparticles have been based on superoxide dismutase, phosphatase, acetylcholine esterase, lactamase, protease, lysozyme, nuclease, thrombin and glucose oxidase.[30–40] Several reports have also described protease assays based on gold nanoparticles.[34,41,42] However, gold nanoparticles have not been used for the detection of ubiquitinating or deubiquitinating enzymes.

We report here a novel method to detect UCH-L1. An artificial UCH-L1 substrate peptide with a ubiquitin moiety was designed with two cysteine amino acids at the two termini. The addition of this peptide caused rapid clustering of the gold nanoparticles, followed by dispersion as a result of the specific cleavage of the substrate peptide by UCH-L1 in a concentration-dependent manner. Under the test conditions, this method can detect clinically reported levels of UCH-L1.

2. Experimental

Purification of recombinant human UCHL-1 and catalytic mutant

Sequences encoding UCH-L1 were amplified from pGEFPC3-hUCH-L1 (a generous gift from Dr Kerstin Brinkmann, University Hospital Cologne, Germany) by PCR and cloned into pRSETA (Invitrogen) for expression in *Escherichia coli* and protein purification. To study the enzymatic role of UCH-L1, the key catalytic residue Cys at position 90 was mutated to Ala by PCR-mediated site-directed mutagenesis. Wild type and mutant UCH-L1 were overexpressed in *E. coli* and purified using Ni-NTA agarose (Qiagen) following the manufacturer's protocol and were further purified by gel filtration using a Superose-12 column (GE Healthcare).

UCHL-1 substrate design

UCHL-1 cleaves the peptide bond present between the C-terminal glycine of ubiquitin and a short peptide, preferably starting with lysine.[43] We therefore modified the ubiquitin molecule with a lysine residue followed by six histidine amino acids and, finally, a cysteine after the C-terminal glycine of ubiquitin (ubiquitin-Lys-6*x*His-Cys). Sequence coding of these residues was introduced by an oligonucleotide primer during PCR amplification of the ubiquitin gene. Ubiquitin with a carboxy-terminal extension was cloned into pRSETA (Invitrogen) for expression in *E. coli* and protein purification. After generating a UCHL-1 substrate with a single-terminal Cys residue, we introduced the second Cys residue at the opposite end of the molecule. The structure of ubiquitin clearly reveals that Lys at position 63 is located exactly opposite to the carboxy-terminus of ubiquitin (Fig. 1A). We mutated this Lys residue to Cys by site-directed mutagenesis and generated a UCH-L1 substrate with two terminal thiol groups. The UCH-L1 substrate was purified by single-step affinity purification using Ni-NTA chromatography as reported previously.[44]

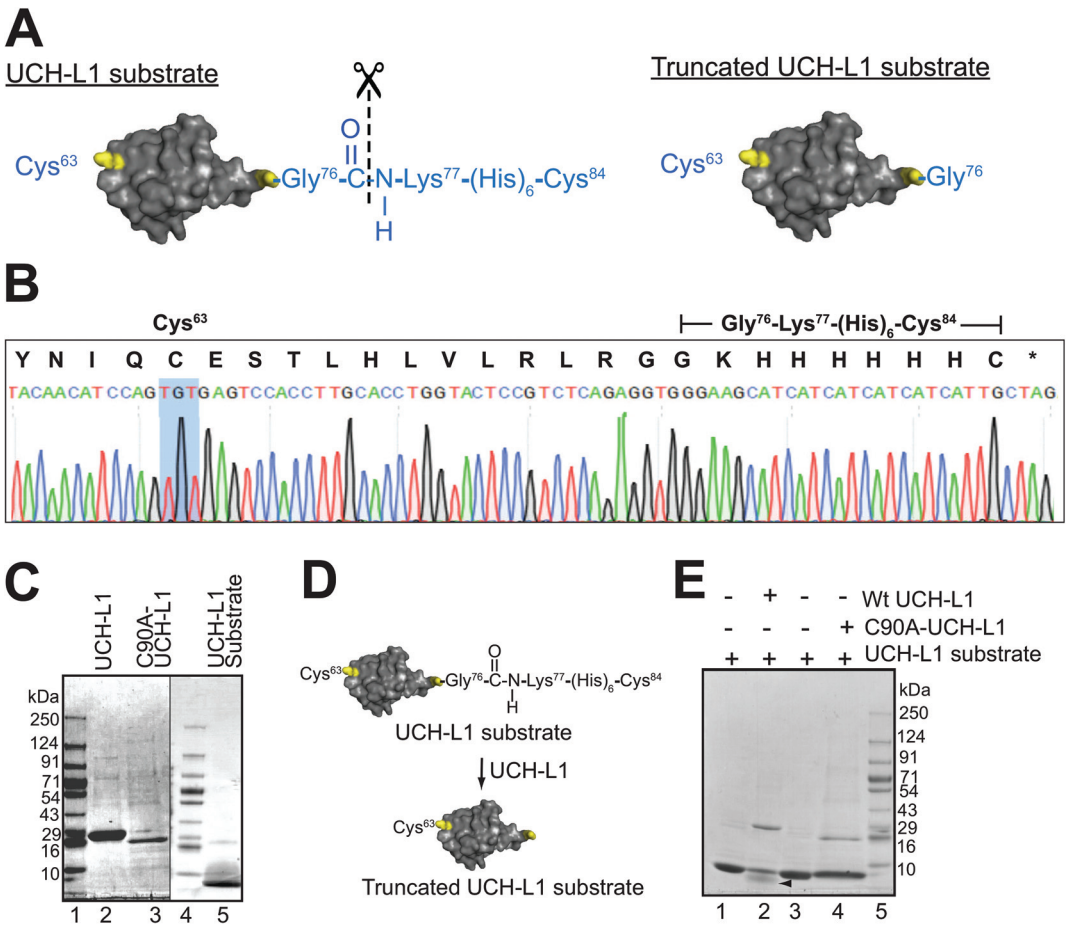

Fig. 1 (A) Design of the UCH-L1 substrate containing two Cys at the two ends. The scissile peptide bond between Gly76 and Lys77 is marked with a dotted line. (B) Sequence analysis of UCH-L1 substrate. Two terminal Cys residues are generated by site-directed mutagenesis. (C) SDS-PAGE analysis of recombinant proteins. His-tag proteins were expressed in *E.coli* cells and purified using Ni-NTA agarose. Proteins were visualized by staining with Coomassie Blue. (D) Outline of cleavage of substrate mediated by UCH-L1. UCH-L1 hydrolyzes the peptide bond between the Gly76 and Lys77 of the substrate peptide and results in a truncated UCH-L1 substrate. (E) SDS-PAGE analysis of proteolytic cleavage by UCH-L1. The purified 9 kDa UCH-L1 substrate (50 μM) was incubated with purified UCH-L1 and C90A mutant UCH-L1 (6.7 μM). Cleavage mediated by UCH-L1was analyzed after 2 h by 4–15% gradient SDS-PAGE followed by Coomassie Blue staining. As a result of partial proteolytic cleavage, both the full-length and the truncated UCH-L1 substrate (8 kDa) were formed. The arrow indicates the position of the truncated substrate.

Purification of UCHL-1 substrate

The UCHL-1 substrate was overexpressed in *E. coli* and purified by single-step affinity purification using Ni-NTA chromatography.[44] Bacterial cells expressing the UCHL-1 substrate were lysed in extraction buffer (50 mM Tris-HCl, pH 8.0, 300 mM sodium chloride, 0.1% Triton-X, 1 mM imidazole). The soluble fraction was then heated for 10 min at 70 °C and the denatured proteins were removed by centrifugation. The recombinant protein was purified using Ni-NTA resin following the manufacturer's protocol.

Enzymatic hydrolysis of C-terminal extension of ubiquitin

The *in vitro* assay of UCH-L1 activity on the ubiquitin substrate was performed by incubating 10 μg (6.7 μM) of UCHL-1 and 25 μg (50 μM) of ubiquitin in 50 μl of reaction buffer containing 20 mM Tris-HCl (pH 8.0), 0.5 mM EDTA, 5 mM DTT and 5% glycerol for 2 h at 30 °C. The cleavage of the ubiquitin C-terminal extension peptide by UCH-L1 was analyzed by gradient (4–15%) SDS-PAGE with Criterion gel (BioRad) using 10 μl of the reaction mix, followed by Coomassie Blue staining.

Synthesis of citrate-capped gold nanoparticles of 30 nm mean diameter

To prepare gold nanoparticles of 30 nm diameter, 0.625 ml of 1% aqueous trisodium citrate and 50 ml of 0.25 mM chloroauric acid ($HAuCl_4$) were refluxed together until the color changed to wine red. The trisodium citrate acted as the reducing agent as well as the stabilizing agent. To confirm the size of the gold nanoparticles, 2.0 μl of a gold nanoparticle solution at a concentration of 0.1 mg ml^{-1} in MilliQ H_2O was dried on a carbon-coated grid and viewed under a Leo 912 AB transmission electron microscope at 120 kV (40 000× magnification). The TEM measurements showed that the size of the nanoparticles was 30 nm. The nanoparticles had a character-

istic absorption peak at 530 nm in the UV–visible spectrum and the concentration was calculated as 0.5×10^{-9} mol L^{-1}.[45]

Aggregation of gold nanoparticles by UCHL-1 substrate

To induce the aggregation of the gold nanoparticles, a 1 : 2000 molar ratio of gold nanoparticles to UCHL-1 substrate (1 μM) was incubated at 37 °C for 30 min in 1 ml of 10 mM citrate buffer at pH 6. The aggregation of the gold nanoparticles was then monitored by UV–visible absorption spectrometry using a U-3900 spectrophotometer (Hitachi). Similar experiments were carried out with ubiquitin containing single-terminal Cys as a negative control.

Dispersion of gold nanoparticles by UCHL-1

To induce the dispersion of the clustered gold nanoparticles, recombinant UCH-L1 was added to the 30 nm gold nanoparticles in the presence of serum in a reaction buffer containing 1 μM UCH-L1 substrate. The UCHL-1 concentration was adjusted to close to the clinically relevant concentration 3.3 nM (100 ng ml^{-1}) and then diluted further to 0.2 ng ml^{-1}. The reaction was then incubated for 2 h at 37 °C for UCH-L1 mediated cleavage to take place. The dispersion of the gold nanoparticles was then monitored by UV–visible absorption spectrophotometry to detect surface plasmon peaks.

Fluorescence-based UCHL-1 assay using Ubiquitin-AMC

Ub-AMC (Sigma) was dissolved in water to make a stock solution with a final concentration of 100 μM. Ub-AMC (5 μM) was mixed with different concentrations of UCH-L1 (0.2–100 ng ml^{-1}) in the presence of serum in a reaction buffer containing 10 mM Tris-HCl (pH 8.0) at 30 °C in a total volume of 300 μl. AMC release was monitored with a Molecular Devices spectrofluorimeter with excitation at 340 nm and emission at 440 nm.

3. Results and discussion

Optimization of UCH-L1 assay

The UCH-L1 substrate was designed with two salient features. The first was a short peptide extension C-terminal to the 76 amino acid ubiquitin protein. To make the substrate specific to UCH-L1, the peptide extension starts with Lys as UCHL-1 preferentially cleaves the peptide bond between the C-terminal Gly residue at position 76 of ubiquitin and the subsequent Lys residue[43] (Fig. 1A). After cleavage with UCH-L1, eight C-terminal amino acid residues are lost and the truncated substrate is about 1 kDa shorter. The peptide extension contains six His residues and a Cys residue at the C-terminus. We designed two Cys residues at the two opposite ends of the molecule to facilitate the aggregation of the gold nanoparticles. The structure of ubiquitin shows that the Lys at position 63 is located opposite to the carboxy-terminus of ubiquitin (PDB entry 1ubq).[46] Therefore, to generate two Cys residues at the head and tail position of the molecule, a Cys residue was added to the C-terminal end and the Lys residue at position 63 was mutated to Cys by site-directed mutagenesis and confirmed by DNA sequencing (Fig. 1B). The recombinant UCH-L1 substrate was overexpressed in *E. coli* cells and purified by Ni-NTA affinity chromatography using the six His residues present in the C-terminal peptide extension (Fig. 1C, lane 5). Recombinant UCH-L1 and UCH-L1 catalytic site mutant (C90A) were also overexpressed and purified from *E. coli* using Ni-NTA affinity chromatography with an N-terminal His-Tag (Fig. 1C, lanes 2 and 3, respectively).

In an effort to demonstrate the deubiquitinase activity of recombinant UCH-L1 using the artificial UCH-L1 substrate *in vitro*, recombinant UCH-L1 was incubated with the UCH-L1 substrate for 2 h. An identical reaction was also carried out with the C90A catalytic mutant of UCH-L1 as a control. The proteolytic cleavage of the ubiquitin C-terminal extension peptide was analyzed by 4–15% SDS-PAGE (Fig. 1D). Wild type UCH-L1 cleaved the eight amino acids extension C-terminal to the ubiquitin moiety, resulting in a truncated UCH-L1 substrate with about a 1 kDa difference in molecular weight (Fig. 1C, lane 2). SDS-PAGE analysis showed that the enzymatic reaction was partially complete as both the full-length and the truncated UCH-L1 substrate were present. Quantitation by image analysis revealed that approximately 40% of the substrate was hydrolyzed. We repeatedly observed such partial proteolysis, even with prolonged incubation, and at present are unable to provide any explanation for this observation. To confirm that the peptide cleavage reaction was specifically due to the enzymatic activity of UCH-L1, we incubated the UCH-L1 substrate with the C90A catalytic mutant of UCH-L1. As expected, C90A UCH-L1 was not able to cleave the substrate peptide and no truncated substrate was detected as a single band on SDS-PAGE (Fig. 1C, lane 4). Together these results suggest that the UCH-L1 substrate could be cleaved by recombinant UCH-L1 *in vitro*.

Aggregation and dispersion of gold nanoparticles

We hypothesized that the UCH-L1 substrate with head and tail Cys thiol groups would trigger the clustering of gold nanoparticles. If active UCH-L1 is then added to these clustered gold nanoparticles, it would cleave the substrate and the gold nanoparticles would disperse again (Fig. 2A). To test this, we synthesized 30 nm citrate-capped gold nanoparticles without any surface modification and confirmed their size by TEM (Fig. 2B). UV–visible absorption spectroscopic analysis revealed a characteristic surface plasmon peak at 530 nm (Fig. 2C, graph a). When the UCH-L1 substrate was added to the gold nanoparticles, complete aggregation was observed in 30 min and a color change from red to purple was seen (Fig. 2C, graph b). We also determined that the minimum concentration of UCH-L1 substrate required to induce the clustering of nanoparticles was 0.25×10^{-6} mol L^{-1} when the gold nanoparticles and UCH-L1 substrate were added in a 1 : 2000 molar ratio. To rule out the possibility of the non-specific aggregation of gold nanoparticles, we mixed UCH-L1 substrate containing a single Cys residue with gold nanoparticles. The UV–visible absorption spectra showed that the peptide containing a single Cys thiol group was unable to induce clustering of the gold nano-

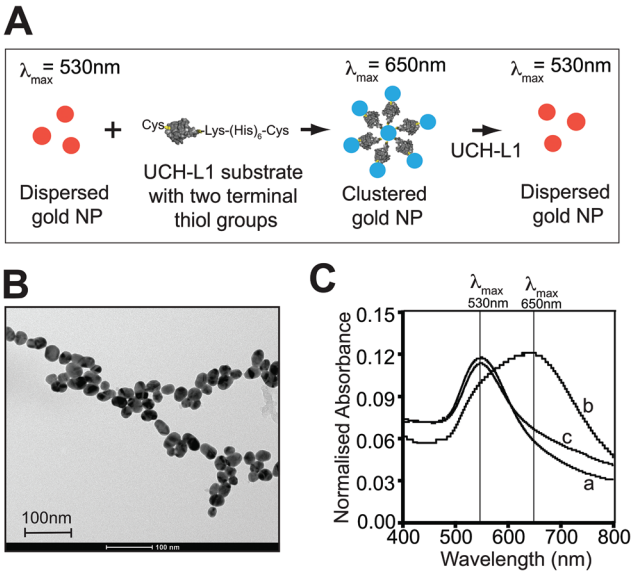

Fig. 2 (A) Outline of gold nanoparticle-based UCH-L1 assay. The addition of the UCH-L1 substrate with two Cys thiol groups triggers the aggregation processes, which can be detected by SPR absorbance at 650 nm. The addition of UCH-L1 cleaves the substrate peptide and disperses the gold nanoparticles, which display SPR absorbance at 530 nm. (B) TEM image of monodispersed citrate-capped gold nanoparticles before aggregation. (C) Absorption spectra of gold nanoparticle solution (0.5 nM in citrate buffer, pH 6.0) in the presence of (a) serum, (b) UCH-L1 substrate (1 μM) with two terminal thiol groups and (c) UCH-L1 substrate with a single thiol group (1 μM).

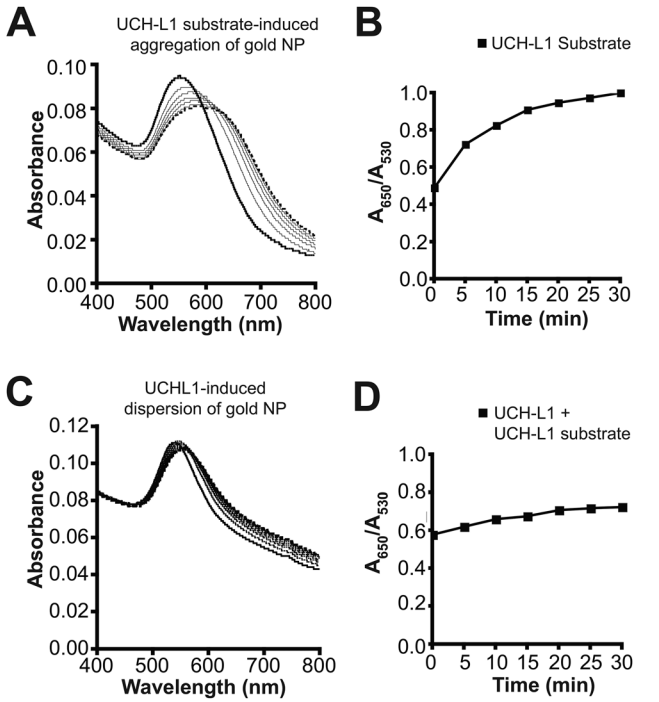

Fig. 3 (A) Change of absorbance in the region 400–800 nm for gold colloids (0.5 nM) on the addition of the UCH-L1 substrate (1 μM) with two Cys thiols (curves taken at 5 min intervals). The dotted line represents the final absorbance profile reached after 30 min. (B) Variation in $A_{650\ nm}/A_{520\ nm}$ *versus* reaction time for the gold nanoparticle solutions containing UCH-L1 substrate peptide (1 μM). (C) Change in the absorbance in the region 400–800 nm for aggregated gold colloids on the addition of UCH-L1 substrate (1 μM) together with UCH-L1 (3.3 nM) (values were recorded at 5 min intervals). The dotted line represents the final absorbance profile reached after 30 min. (D) Variation of $A_{650\ nm}/A_{520\ nm}$ *versus* reaction time for the gold nanoparticle solutions containing UCH-L1 substrate peptide (1 μM) in the presence of 100 ng ml^{-1} (3.3 nM) UCH-L1.

particles (Fig. 2C, graph c). These results suggested that the aggregation of nanoparticles was specifically due to the two terminal Cys thiols present in the UCH-L1 substrate.

We then analyzed the time course of UCH-L1 substrate-induced aggregation by monitoring the change in absorption. As shown in Fig. 3A, the absorption at 650 nm (A_{650}) gradually increased and the absorption at 530 nm (A_{530}) decreased in the presence of the UCH-L1 substrate, suggesting a shift in plasmonic resonance as a result of the formation of aggregates. To demonstrate this more clearly, the A_{650}/A_{530} ratio was plotted against time (Fig. 3B). An increase in the fraction of aggregated gold nanoparticles caused a gradual increase in the A_{650}/A_{530} ratio. To test whether UCH-L1 mediated cleavage of its substrate would inhibit the aggregation of gold nanoparticles, the UCH-L1 substrate was added to the gold nanoparticles in the presence of recombinant UCH-L1 and the spectral changes were recorded. The addition of UCH-L1 prevented aggregate formation and no increase in absorption was observed at 650 nm (Fig. 3C). This was probably a result of the lack of availability of the substrate peptide due to proteolytic cleavage by UCH-L1. As expected, we observed that the ratio of A_{650}/A_{530} *versus* time remained almost unchanged (Fig. 3D). The small increase in A_{650}/A_{530} may be due to partial cleavage of the UCH-L1 substrate. We also aggregated the gold nanoparticles and carried out UCH-L1 mediated dispersion of the aggregated nanoparticles in the presence of serum to mimic clinical samples or bacterial or HeLa cell extracts that do not express endogenous UCH-L1. We observed that the aggregation or dispersion of gold nanoparticles was not affected as a result of the presence of serum or cellular proteins and the results were identical to Fig. 3A and B.

We then studied the time course of UCH-L1-induced dispersion of the aggregated gold nanoparticles in the presence of serum, bacterial cell extracts or HeLa cell extracts. We observed that the A_{650}/A_{530} ratio also remained unchanged (as in Fig. 3C and D), suggesting that the presence of serum or cellular proteins had no effect on the UCH-L1 induced dispersion of nanoparticle aggregates. To rule out cleavage of the substrate by any non-specific proteases, we performed the gold nanoparticle dispersion assay using mutant C90A UCH-L1. As expected, the A_{650}/A_{530} ratio also remained unchanged in the presence of mutant C90A UCH-L1 (ESI, Fig. S2A†). We also tested the substrate cleavage by adding the non-specific protease trypsin. Trypsin cleaves peptide bond carboxyl termini to lysine and arginine. The UCH-L1 peptide substrate contains ubiquitin followed by an eight amino acid extension starting with lysine. As ubiquitin itself has seven lysine and nine arginine residues, adding trypsin would cleave ubiquitin itself at

multiple positions, in addition to the lysine present at the C-terminus to Gly 76 of ubiquitin (Fig. S2B†).

Fluorescence-based detection of UCHL-1 activity

The only available functional assay reported for UCH-L1 is based on the hydrolysis of the artificial UCH-L1 substrate Ub-AMC (Fig. 4A).[47] We first wanted to determine the efficiency of the Ub-AMC hydrolysis assay for the detection of the presence of UCH-L1 using recombinant protein. Purified UCH-L1 mediated hydrolysis of Ub-AMC resulted in the release of AMC, which showed a peak absorption at 340 nm and emission at 440 nm (Fig. 4B, graph b). No background fluorescence was detected in the absence of UCH-L1 (Fig. 4B, graph a). We wanted to test the efficiency of UCH-L1 detection based on Ub-AMC in clinical samples. We hydrolyzed Ub-AMC with UCH-L1 in the presence of serum to mimic clinical samples. When Ub-AMC was incubated with UCH-L1 in the presence of serum, AMC hydrolysis resulted in a distinct fluorescence emission peak 440 nm (Fig. 4C, graph b). When UCH-L1 was omitted in the reaction mixture, the fluorescence emission peak at 440 nm was still observed (Fig. 4C, graph a). This fluorescence emission at 440 nm (Fig. 4C, graph a) was completely absent in the serum-free samples (Fig. 4B, graph a). This suggested that the presence of serum contributed a high background fluorescence.

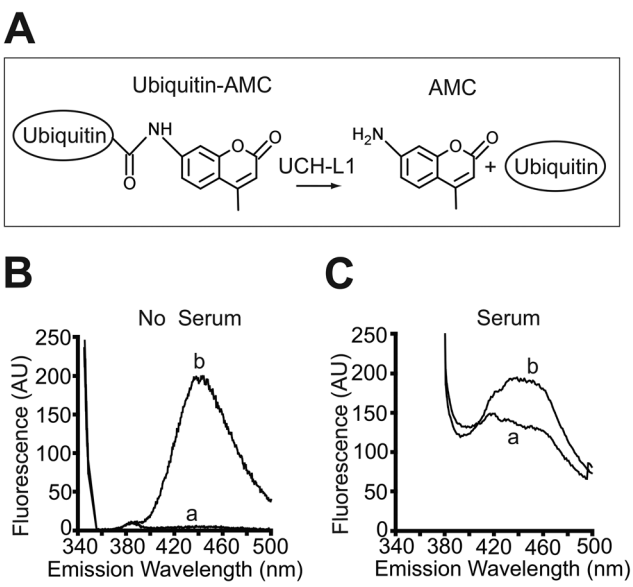

Fig. 4 (A) Schematic representation of the method for assaying UCH-L1 using Ubiquitin-AMC. Ub-AMC (5 μM) was mixed with UCH-L1 (100 ng ml^{-1} or 3.3 nM) in the presence and absence of serum and the release of AMC was monitored with excitation at 340 nm and emission at 440 nm. (B) Emission spectra showing the increase in fluorescence with cleavage of the peptide bond by UCH-L1. Graph (a) represents the background fluorescence in the absence of UCH-L1. (C) Emission spectra showing the increase in fluorescence on cleavage of the peptide bond by UCH-L1 in the presence of serum (b). Graph (a) shows the background fluorescence in the absence of UCH-L1 in the presence of serum.

Comparison of sensitivity of the nanoparticle-based and the fluorescence-based methods

To compare the sensitivity of the nanoparticle-based and fluorescence-based methods for detecting functional UCH-L1, we performed the UCH-L1 assay using a range of UCH-L1 concentrations in the absence and presence of serum. The concentration range of UCH-L1 used in these reactions (1.8–100 ng ml^{-1} UCH-L1) was decided by the amount of UCH-L1 released into blood serum after brain injury (2–50 ng ml^{-1}).[15] We first tested whether diluted UCH-L1 in the samples causes the dispersion of gold nanoparticles. We observed that concentrations of UCH-L1 as low as 20 ng ml^{-1} resulted a significant change in the A_{650}/A_{530} ratio (Fig. 5A). The presence of serum did not influence the detection limit (Fig. 5A and S1†). We also performed UCHL-1 catalyzed hydrolysis of Ub-AMC with a similar range of concentrations of UCHL-1 in the absence of serum. As shown in Fig. 5B, the presence of serum resulted in high background fluorescence and a poor detection limit, especially when UCH-L1 was present at lower concentrations. A high background fluorescence as a result of the presence of plasma proteins impeded the accurate detection of UCH-L1 in the range 25–100 ng ml^{-1} (Fig. 5B). In contrast, the UCH-L1 detection assay based on gold nanoparticles was sensitive to 10–100 ng ml^{-1} of UCH-L1, even in the presence of serum or cell extracts in the assay mixture (Fig. 5A and S1†). Furthermore, the assay based on SPR absorbance was superior with respect to a lower limit of detection and the upper limit of quantification. The slope of a linear regression analysis graph was large enough to differentiate between small changes in UCH-L1 concentration (Fig. 5A). In contrast, the calibration graph derived from Ub-AMC hydrolysis did not show a linear region in the presence of serum, whereas the fluorescence varies linearly with UCH-L1 concentration (Fig. 5B). The calibration graph obtained using the assay based on gold nano-

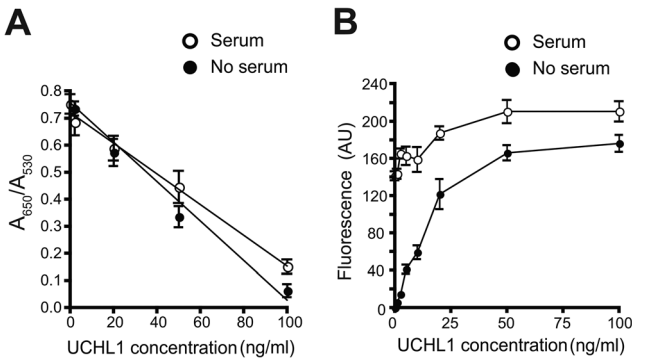

Fig. 5 Calibration graph for the determination of UCH-L1 concentration. (A) 30 nm gold nanoparticles (0.5 nM) and UCH-L1 substrate with two terminal thiol groups (1 μM) were mixed with various concentrations of UCH-L1 in the absence or presence of serum for 2 h. The calibration graph was obtained by plotting the variation of $A_{650\ nm}/A_{530\ nm}$ *versus* UCH-L1 concentration. (B) Ub-AMC (5 μM) was mixed with different concentrations of UCH-L1 in the absence or presence of serum and the calibration graph was obtained by plotting the fluorescence emission (440 nm) against UCH-L1 concentration.

particles could be used to detect UCH-L1 at least two orders of magnitude lower than calibration graph obtained using the fluorescence-based assay. Together these results suggest that the assay described here is better in terms of detection limit, sensitivity, simplicity and lack of interference from cellular or plasma proteins. Given the growing role of UCH-L1 in neurodegenerative disorders and cancer, we anticipate that this simple assay will be useful in the high-throughput screening of inhibitors. Moreover, the design of the ubiquitin-peptide substrate described here could be tailored to assay other UCHs.

4. Conclusion

This UCH-L1 assay based on gold nanoparticles can be used to detect functional UCH-L1 *in vitro via* the hydrolysis of a short peptide containing ubiquitin. The sensitivity is enhanced compared with the presently available fluorescence-based assay. The fluorescence-based assay using the hydrolysis of Ub-AMC for the detection of UCH-L1 is affected by high background fluorescence and therefore is not sensitive. Our nanoparticle-based assay does not require nanoparticle functionalization and UCHL-1 can be detected by a simple analysis of SPR absorbance, even in the presence of plasma proteins or cell extracts. The assay may be useful for detecting UCH-L1 in clinical samples to determine the severity of brain injury. The assay is also suitable for the high-throughput screening of UCH-L1 inhibitors to elucidate the etiological role of UCH-L1 in Parkinson's disease and some cancers.

Acknowledgements

This work was funded by the Department of Biotechnology (DBT), Government of India (Project no. 102/IFD/SAN/634/2013–2014; DT 09-05-2013).

Notes and references

1 J. P. Cata, B. Abdelmalak and E. Farag, *Br. J. Anaesth.*, 2011, **107**, 844–858.
2 P. Jackson and R. J. Thompson, *J. Neurol. Sci.*, 1981, **49**, 429–438.
3 B. Gong and E. Leznik, *Drug News Perspect*, 2007, **20**, 365–370.
4 S. B. Lewis, R. Wolper, Y. Y. Chi, L. Miralia, Y. Wang, C. Yang and G. Shaw, *J. Neurosci. Res.*, 2010, **88**, 1475–1484.
5 P. K. Dash, J. Zhao, G. Hergenroeder and A. N. Moore, *Neurotherapeutics*, 1997, **7**, 100–114.
6 R. P. Berger, S. R. Beers, R. Richichi, D. Wiesman and P. D. Adelson, *J. Neurotrauma*, 2007, **24**, 1793–1801.
7 Y. Yamazaki, K. Yada, S. Morii, T. Kitahara and T. Ohwada, *Surg. Neurol.*, 1995, **43**, 267–270; discussion 270–261.
8 S. A. Ross, R. T. Cunningham, C. F. Johnston and B. J. Rowlands, *Br. J. Neurosurg.*, 1996, **10**, 471–476.
9 U. Missler, M. Wiesmann, C. Friedrich and M. Kaps, *Stroke*, 1997, **28**, 1956–1960.
10 I. N. Day and R. J. Thompson, *Prog. Neurobiol.*, 1997, **90**, 327–362.
11 D. T. Laskowitz, H. Grocott, A. Hsia and K. R. Copeland, *J. Stroke Cerebrovasc Dis.*, 1998, **7**, 234–241.
12 P. Martens, *Acad Emerg Med*, 1996, **3**, 126–131.
13 M. C. Liu, L. Akinyi, D. Scharf, J. Mo, S. F. Larner, U. Muller, M. W. Oli, W. Zheng, F. Kobeissy, L. Papa, X. C. Lu, J. R. Dave, F. C. Tortella, R. L. Hayes and K. K. Wang, *Eur J Neurosci*, 2010, **31**, 722–732.
14 S. Mondello, A. Linnet, A. Buki, S. Robicsek, A. Gabrielli, J. Tepas, L. Papa, G. M. Brophy, F. Tortella, R. L. Hayes and K. K. Wang, *Neurosurgery*, 2012, **70**, 666–675.
15 G. M. Brophy, S. Mondello, L. Papa, S. A. Robicsek, A. Gabrielli, J. Tepas 3rd, A. Buki, C. Robertson, F. C. Tortella, R. L. Hayes and K. K. Wang, *J. Neurotrauma*, 2011, **28**, 861–870.
16 L. Papa, L. Akinyi, M. C. Liu, J. A. Pineda, J. J. Tepas 3rd, M. W. Oli, W. Zheng, G. Robinson, S. A. Robicsek, A. Gabrielli, S. C. Heaton, H. J. Hannay, J. A. Demery, G. M. Brophy, J. Layon, C. S. Robertson, R. L. Hayes and K. K. Wang, *Crit. Care Med.*, 2010, **38**, 138–144.
17 K. D. Wilkinson, K. M. Lee, S. Deshpande, P. Duerksen-Hughes, J. M. Boss and J. Pohl, *Science*, 1989, **246**, 670–673.
18 K. Hibi, Q. Liu, G. A. Beaudry, S. L. Madden, W. H. Westra, S. L. Wehage, S. C. Yang, R. F. Heitmiller, A. H. Bertelsen, D. Sidransky and J. Jen, *Cancer Res.*, 1998, **58**, 5690–5694.
19 Y. Miyoshi, S. Nakayama, Y. Torikoshi, S. Tanaka, H. Ishihara, T. Taguchi, Y. Tamaki and S. Noguchi, *Cancer Sci.*, 2006, **97**, 523–529.
20 T. Otsuki, K. Yata, A. Takata-Tomokuni, F. Hyodoh, Y. Miura, H. Sakaguchi, T. Hatayama, S. Hatada, T. Tsujioka, Y. Sato, H. Murakami, Y. Sadahira and T. Sugihara, *Br. J. Haematol.*, 2004, **127**, 292–298.
21 T. Takano, A. Miyauchi, F. Matsuzuka, H. Yoshida, Y. Nakata, K. Kuma and N. Amino, *Eur. J. Cancer*, 2004, **40**, 614–618.
22 T. Yamazaki, K. Hibi, T. Takase, E. Tezel, H. Nakayama, Y. Kasai, K. Ito, S. Akiyama, T. Nagasaka and A. Nakao, *Clin. Cancer Res.*, 2002, **8**, 192–195.
23 E. Tezel, K. Hibi, T. Nagasaka and A. Nakao, *Clin. Cancer Res.*, 2000, **6**, 4764–4767.
24 R. M. Mohammad, A. Maki, G. R. Pettit and A. M. al-Katib, *Enzyme Protein*, 1996, **49**, 262–272.
25 H. Sasaki, H. Yukiue, S. Moriyama, Y. Kobayashi, Y. Nakashima, M. Kaji, I. Fukai, M. Kiriyama, Y. Yamakawa and Y. Fujii, *Jpn. J. Clin. Oncol.*, 2001, **31**, 532–535.
26 T. Y. Yanagisawa, Y. Sasahara, H. Fujie, Y. Ohashi, M. Minegishi, M. Itano, S. Morita, S. Tsuchiya, Y. Hayashi, R. Ohi and T. Konno, *J. Exp. Med.*, 1998, **184**, 229–240.
27 A. Leiblich, S. S. Cross, J. W. Catto, G. Pesce, F. C. Hamdy and I. Rehman, *Prostate*, 2007, **67**, 1761–1769.
28 Y. Liu, H. A. Lashuel, S. Choi, X. Xing, A. Case, J. Ni, L. A. Yeh, G. D. Cuny, R. L. Stein and P. T. Lansbury Jr., *Chem. Biol.*, 2003, **10**, 837–846.

29 C. Guarise, L. Pasquato and P. Scrimin, *Langmuir*, 2005, **21**, 5537–5541.
30 S. Hong, I. Choi, S. Lee, Y. I. Yang, T. Kang and J. Yi, *Anal. Chem.*, 2009, **81**, 1378–1382.
31 Y. Choi, N. H. Ho and C. H. Tung, *Angew. Chem., Int. Ed.*, 2007, **46**, 707–709.
32 M. Wang, X. Gu, G. Zhang, D. Zhang and D. Zhu, *Langmuir*, 2009, **25**, 2504–2507.
33 R. Liu, R. Liew, J. Zhou and B. Xing, *Angew, Chem., Int. Ed*, 2007, **46**, 8799–8803.
34 C. Guarise, L. Pasquato, V. De Filippis and P. Scrimin, *Proc. Natl. Acad. Sci. U. S. A.*, 2006, **103**, 3978–3982.
35 Z. Wang, R. Levy, D. G. Fernig and M. Brust, *J. Am. Chem. Soc.*, 2006, **128**, 2214–2215.
36 A. Laromaine, L. Koh, M. Murugesan, R. V. Ulijn and M. M. Stevens, *J. Am. Chem. Soc.*, 2007, **129**, 4156–4157.
37 Y. C. Chuang, J. C. Li, S. H. Chen, T. Y. Liu, C. H. Kuo, W. T. Huang and C. S. Lin, *Biomaterials*, 2010, **31**, 6087–6095.
38 Y. M. Chen, C. J. Yu, T. L. Cheng and W. L. Tseng, *Langmuir*, 2008, **24**, 3654–3660.
39 X. Xu, M. S. Han and C. A. Mirkin, *Angew. Chem., Int. Ed.*, 2007, **46**, 3468–3470.
40 P. Pandey, S. P. Singh, S. K. Arya, V. Gupta, M. Datta, S. Singh and B. D. Malhotra, *Langmuir*, 2007, **23**, 3333–3337.
41 G. B. Kim, K. H. Kim, Y. H. Park, S. Ko and Y. P. Kim, *Biosens. Bioelectron.*, 2013, **41**, 833–839.
42 C. K. Chen, C. C. Huang and H. T. Chang, *Biosens. Bioelectron.*, 2010, **25**, 1922–1927.
43 C. N. Larsen, B. A. Krantz and K. D. Wilkinson, *Biochemistry*, 1998, **37**, 3358–3368.
44 R. Anindya, P. O. Mari, U. Kristensen, H. Kool, G. Giglia-Mari, L. H. Mullenders, M. Fousteri, W. Vermeulen, J. M. Egly and J. Q. Svejstrup, *Mol. Cell*, 2010, **38**, 637–648.
45 X. Liu, M. Atwater, J. Wang and Q. Huo, *Colloids Surf., B*, 2007, **58**, 3–7.
46 S. Vijay-Kumar, C. E. Bugg and W. J. Cook, *J. Mol. Biol.*, 1987, **194**, 531–544.
47 A. Case and R. L. Stein, *Biochemistry*, 2006, **45**, 2443–2452.